DESIGN OF A MULTISTAGE MAGNETIC GEAR FOR HYDRO APPLICATIONS

Kang Li[1]
Electrical and Computer Engineering
University of North Carolina at Charlotte
Charlotte, NC, USA

Jonathan Z. Bird
Electrical and Computer Engineering
Portland State University
Portland, OR, USA

[1]Corresponding author: kang.li@ieee.org

INTRODUCTION

Hydropower is the most widely used renewable source of energy which is nonpolluting. It is of great importance to improve the efficiency and reliability of the generators. Most of the hydropower generators utilize either a direct-drive synchronous generator or a mechanical gearbox coupled to a generator. The direct-drive synchronous generator typically cannot achieve a torque density greater than 50 Nm/L [1-3]. Whilst the use of a mechanical gearbox will reduce the reliability significantly and increase the cost.

A magnetic gearbox (MG), has the potential to operate with high reliability, high efficiency whilst also being compact in size [4-6]. It may be a good choice for improving hydro power generation. As the MG does not need lubrication it could also help to reduce the risk of water lubrication pollution [7]. This paper discusses the design and optimization of a 50 kW small hydro multistage magnetic gear (MSMG) with a high gear ratio. The MSMG is designed to be competitive with an equivalent 59:1 mechanical gearbox (Sumitomo CHHJ-4225Y-59-320TC).

PRINCIPLES OF THE MULTISTAGE MAGNETIC GEAR

In order to achieve a high gear ratio two MG stages connected in series will be utilized. Each stage uses the co-axial flux focusing topology which is shown in Figure 1.

For the stage 1 MG, the inner rotor (rotor 1) has p_1 pole-pairs with an angular speed, ω_1, the cage rotor (rotor 2) has n_2 pole-pairs with an angular speed, ω_2, and the outer rotor (rotor 3) has p_3 pole-pairs with an angular speed ω_3.

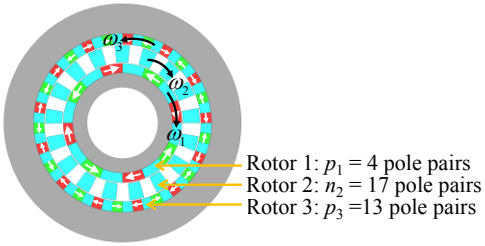

FIGURE 1. CO-AXIAL MAGNETIC GEARBOX EXAMPLE.

In order to maximize coupling between rotors the pole-pairs must be selected such that

$$n_2 = p_1 + p_3 \quad (1)$$

and then the angular speed relationship will be:

$$p_1\omega_1 + p_3\omega_3 = n_2\omega_2 \quad (2)$$

If the outer rotor is fixed as a stationary part ($\omega_3 = 0$). Then Equation 2 becomes:

$$p_1\omega_1 = n_2\omega_2 \quad (3)$$

The stage 1 gear ratio is then:

$$G_{12} = \omega_1 / \omega_2 = n_2 / p_1 = (p_1 + p_3) / p_1 \quad (4)$$

The stage 2 MG uses the same typology as the stage 1 MG (as shown in Figure 1). The inner rotor (rotor 4), cage rotor (rotor 5) and outer rotor (rotor 6) have p_4, n_5 and p_6 pole pairs. The speed and the number of pole pairs are then related by:

$$n_5 = p_4 + p_6 \quad (5)$$

$$n_5\omega_5 = p_4\omega_4 + p_6\omega_6 \quad (6)$$

where ω_4, ω_5 and ω_6 are the angular speed of the inner, cage and outer rotors, respectively. The outer rotor of stage 2 MG is fixed ($\omega_6 = 0$). Then the gear ratio of stage 2 is calculated by:

$$G_{45} = n_5 / p_4 \quad (7)$$

With rotor 1 and rotor 5 connected such that $\omega_1 = \omega_5$ then the gear ratio of the MSMG will be:

$$G_r = G_{12}G_{45} = (n_2 n_5) / (p_1 p_4) \quad (8)$$

DESIGN OF STAGE 1 MG

The pole pair combination of the stage 1 MG was chosen to be p_1 = 12, n_2 = 78 and p_3 = 66. From Equation 4, this gives a gear ratio of G_{12} =6.5. This gear ratio can be simulated with a 1/6 partial model which is shown in Figure 2. In this study the outer radius was fixed at r_{o3} = 270 mm, which is close to the outer radii of the Sumitomo mechanical gearbox. The axial length was fixed at d_1= 75 mm and the air gap was g = 1 mm. Table I shows the active material used in this study. In the following analysis the outer and inner magnet angular lengths were kept equal to the steel lengths:

$$\theta_{1m} = \theta_{1s} \quad (9)$$

$$\theta_{3m} = \theta_{3s} \quad (10)$$

where subscript m and s denote magnet and steel parts. These angles are defined in Figure 2.

$$\theta_{2s} = 2\theta_{3s} \quad (11)$$

In this paper 2-D electromagnetic finite element analysis has been used to study the performance of the MG. A judicious parameter sweep analysis was used. This work draws upon prior work [8]. Considering the design shown in Figure 2 the inner radius of the inner rotor, r_{i1}, the outer radius of the inner rotor, r_{o1}, the radial length of the cage rotor, l_2 and the inner radius of the outer rotor, r_{i3} were all varied in order to obtain the peak torque. A mass and volume torque densities plot for each geometric parameter is shown in Figure 3.

TABLE I. MATERIALS USED IN THE MG ANALYSIS.

Steel teeth	M19 lamination
Steel rods	Steel 416
Plastic rods and bars	Carbon fiber
Magnets	NMX 40CH

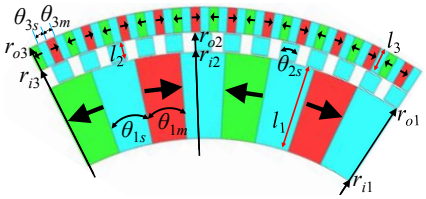

FIGURE 2. A 1/6 PARTIAL MODEL OF STAGE 1 MG.

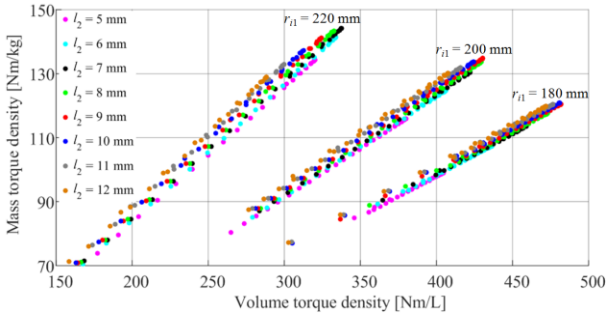

FIGURE 3. MASS AND VOLUME TORQUE DENSITIES WITH DIFFERENT VALUES OF R_{I1}.

For different values of r_{i1}, the torque density values are grouped. When l_2 is increased, the torque densities will increase and then decrease.

The inner radius of the inner rotor r_{i1} was varied from 150 mm to 240 mm. At each value of r_{i1}, the peak torque was obtained. The torque density plots are shown in Figure 4. Figure 4 shows that when varying r_{i1} there is a clear tradeoff between maximizing volume torque density and the mass torque density. The value of r_{i1} was chosen to be 180 mm to achieve a relatively high volume torque density (smaller r_{i1} value will result in too large a size of inner magnets which will increase the assembly difficulty [8]). In order to make the MG mechanically strong enough (small deflection of the cage rotor) while still achieving a relatively high torque, l_2 was chosen as 15 mm. Then with r_{i1} and l_2 fixed, r_{o1} was again varied from 220 mm to 250 mm. The peak torque occurs when r_{o1} = 236 mm which is shown in Figure 5. The corresponding active region volume and mass torque densities are 434.85 Nm/L and 112.13 Nm/kg, respectively.

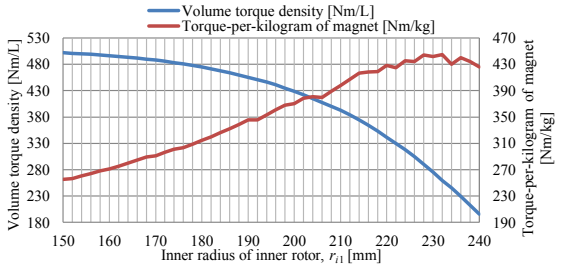

(a)

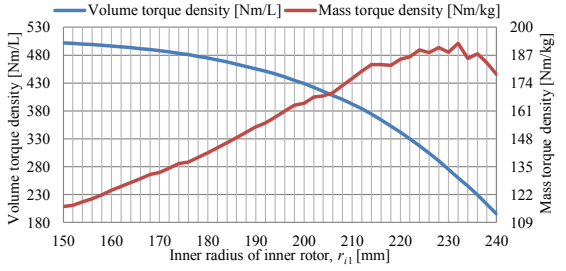

(b)

FIGURE 4. VOLUME AND (A) MAGNET MASS TORQUE DENSITIES (B) MASS TORQUE DENSITIES.

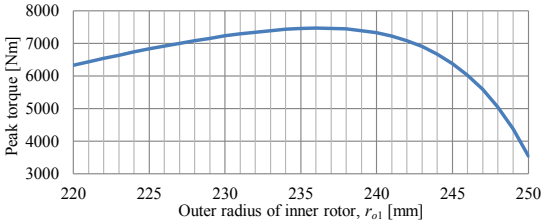

FIGURE 5. PEAK TORQUE WHEN R_{O1} WAS VARIED.

Rods and retaining lips have been added to the stage 1 MG design which is shown in Figure 6 (a). The peak cage rotor torque then reduces to T_2 = 6113 Nm. To achieve a higher torque, radial magnets were added into the inner rotor to make it flux concentrating [9] as shown in Figure 6 (b).

The radial length of the radial magnets was then varied to obtain the peak torque. The peak torque occurs when the radial length is 17 mm as shown in Figure 7. The calculated torque increased to T_2 = 6559 Nm which gives a volume torque density of 370 Nm/L. The final parameters for the stage 1 design (shown in Figure 6 (b)) are given in Table II. The radial force on one single cage bar is shown in Figure 8. The torque at peak condition on the cage rotor is present in Figure 9. The torque ripple is 0.35 %. The efficiency calculated using the 2-D FEA is 95 % when the cage rotor operating at 80 RPM. The loss density is shown in Figure 10. Most losses are from the outer rotor.

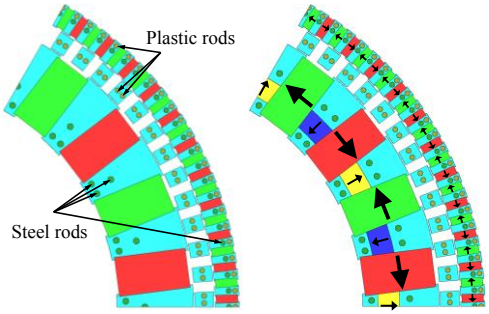

FIGURE 6. (A) STAGE 1 MG WITH RODS AND (B) FINAL DESIGN OF STAGE 1 MG.

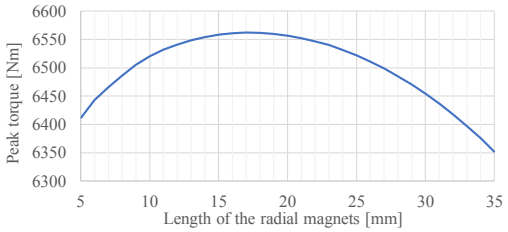

FIGURE 7. PEAK TORQUE WITH DIFFERENT RADIAL LENGTH OF THE INNER RADIAL MAGNETS.

TABLE II. GEOMETRY PARAMETERS OF STAGE 1 MG.

Description		Value	Unit
Inner rotor	Inner radius, r_{i1}	178	mm
	Outer radius, r_{o1}	238	mm
Cage rotor	Inner radius, r_{i2}	239	mm
	Outer radius, r_{o2}	254	mm
Outer rotor	Inner radius, r_{i3}	255	mm
	Outer radius, r_{o3}	274	mm
Axial length, d_1		75	mm
Air gap, g		1	mm

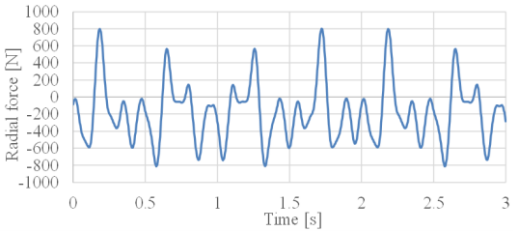

FIGURE 8. RADIAL FORCE ON ONE CAGE BAR.

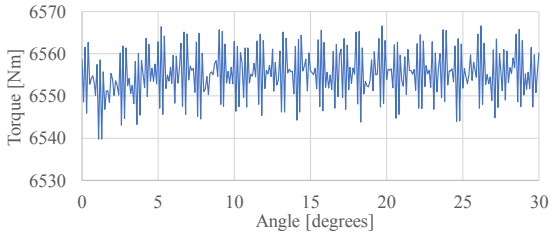

FIGURE 9. LOW SPEED CAGE ROTOR TORQUE.

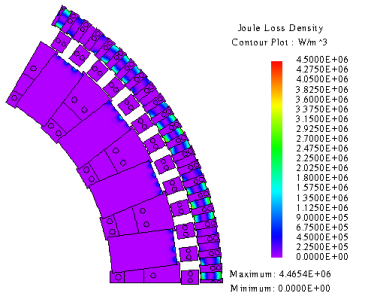

FIGURE 10. LOSS DENSITY OF THE STAGE 1 MG.

DESIGN OF STAGE 2 MG

The pole-pair combination of the stage 2 MG was chosen as p_4 = 6, n_5 = 57 and p_6 = 51. This gives a stage 2 gear ratio of G_{45} = 9.5. Using this pole combination, a 1/3 partial model can be simulated due to symmetry. From Equation 8 the overall gear ratio is G_r = 61.75. The parameters for the stage 2 design are defined in Figure 11. The axial length of the stage 2 MG was fixed at d_2 = 37.5 mm. The inner radius of the inner rotor was fixed at r_{i4} = 155 mm so that a stator could be put inside in the future. The radial length of the cage rotor was fixed at 15 mm so that the steel could provide enough mechanical support to prevent deflection.

The radial length of the inner and outer magnets is defined as $l_4 = r_{o4} - r_{i4}$ and $l_6 = r_{o6} - r_{i6}$. The inner magnet length was varied from l_4 = 35 mm to 60 mm and the outer magnets were varied from l_6 = 10 mm to 40 mm. The parameter sweep result is shown in Figure 12.

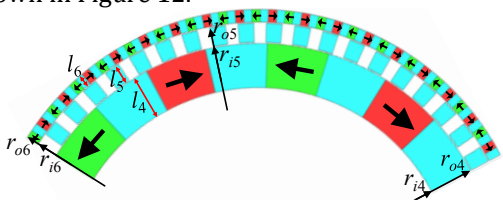

FIGURE 11. A 1/3 PARTIAL MODEL OF STAGE 2 MG.

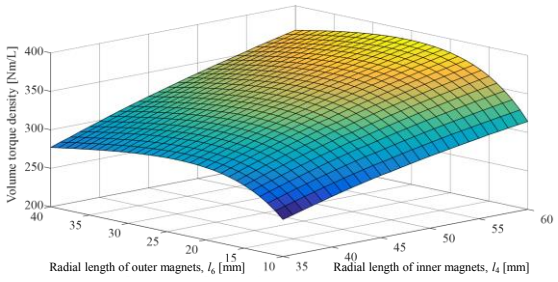

FIGURE 12. PARAMETER SWEEP OF STAGE 2 MG.

From Figure 12 the volume torque density is increasing when the radial length of the inner magnets is increasing. Using too large an inner magnet will increase the cost, weight and assembly difficulty. Therefore, the inner radial length was selected to be l_4 = 45 mm. To achieve the peak torque density, the outer radial length was l_6 = 24 mm.

Similar to the stage 1 MG, the radial magnets were added to the inner rotor of the stage 2 MG as shown in Design 1 of Table III. The peak torque occurred when the radial length of the radial magnets was l_{m4} = 20 mm. Radial magnets, 4.5 by 5 mm in size were also added to the outer rotor.

The performance of a series of alternative designs has also been compared as shown in Table III. These designs try to look at how the mechanical and magnetic performance is traded-off to create a robust and realistic design with a high torque density. Though Design 1 has the highest torque value, it has many steel rods on the outer rotor which increase losses. The efficiency is also only 79 % (at cage rotor angular speed ω_4 = 195 RPM). Design 2 has no outer steel rods and the non-magnetic rods may not provide sufficient support. Design 3 has a low torque. In design 5, each cage bar has one single rod and there is rectangular Garolite bar between cage segments. The cage rods have also been changed to be round, improving manufacturability. Design 6 is the final design as the torque is higher than that in Design 5. The calculated torque density is 344 Nm/L and the final parameters are shown in Table IV. The radial force on one cage bar for Design 6 is shown in Figure 13. The torque on the cage rotor is present in Figure 14 and the torque ripple is 0.28 %. Using 2-D FEA the efficiency was calculated to be 89 % at ω_4 = 520 RPM. The loss density is plotted in Figure 15. Most of the losses are associated with the outer magnets because of the higher frequency. These losses could be greatly mitigated by axially segmenting the magnets.

TABLE III. COMPARISON OF DIFFERENT DESIGNS.

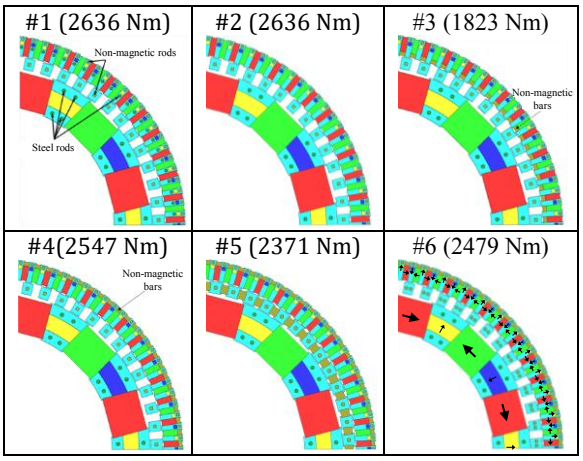

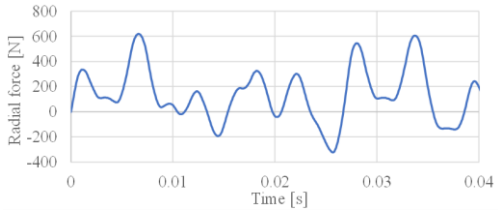

FIGURE 13. RADIAL FORCE ON ONE CAGE BAR.

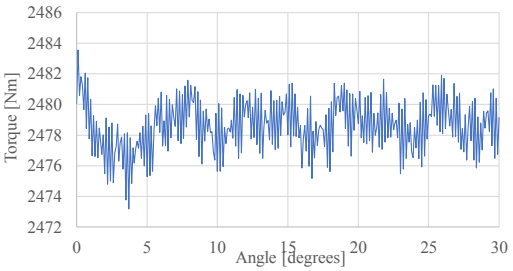

FIGURE 14. TORQUE ON THE CAGE ROTOR.

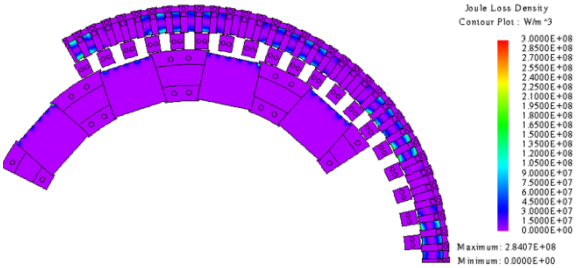

FIGURE 15. LOSS DENSITY OF THE STAGE 2 MG.

TABLE IV. GEOMETRY PARAMETERS OF STAGE 2 MG.

Description			Unit
Inner rotor	Inner radius, r_{i4}	155	mm
	Outer radius, r_{o4}	204	mm
Cage rotor	Inner radius, r_{i5}	205	mm
	Outer radius, r_{o5}	220	mm
Outer rotor	Inner radius, r_{i6}	221	mm
	Outer radius, r_{o6}	247	mm
Axial length, d_2		37.5	mm
Air gap, g		1	mm

DESIGN OF STAGE 2 MG WITH STATOR

A stator has been added inside the inner rotor of the stage 2 MG. The stator will create 12 poles so that it can generate a constant torque. A 45-slot stator was designed which is shown in Figure 16. The distribution of the three-phase distributed winding (phase U, phase W and phase V) is also shown in Figure 16 for a 1/3 model.

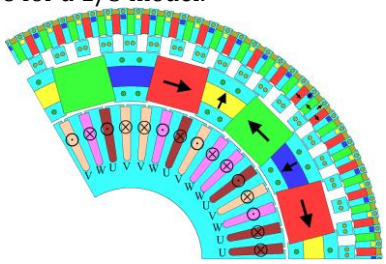

FIGURE 16. STAGE 2 MG WITH 45-SLOT STATOR.

The number of turns in each coil is N_t and the turns function is $n(\theta)$ which gives the total number of turns in a span of θ. The winding function $N(\theta)$, is related to the turns function by [10]

$$N(\theta) = n(\theta) - < n(\theta) > \quad (12)$$

where $<n(\theta)>$ is the average of the turns function. The winding functions are shown in Figure 17 (a)-(c). When $I_W = I_V = -0.5I_U$, the combined winding function is shown in Figure 17 (d). It can be clearly seen that 12 poles (6 pole pairs) is created.

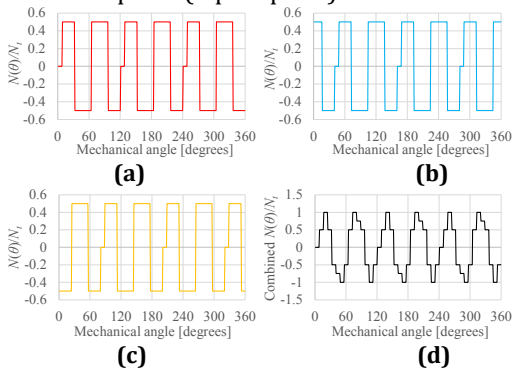

FIGURE 17. THE WINDING FUNCTION FOR (A) PHASE U (B) PHASE W (C) PHASE V AND (D) COMBINED.

The phase of the winding was chosen to achieve the highest torque and the corresponding torque on the inner rotor is plotted in Figure 18 with a torque ripple of 5.6 %. The parameters of the stator are shown in Table V.

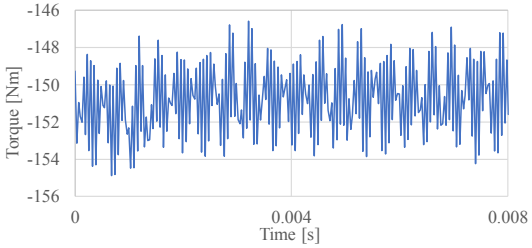

FIGURE 18. TORQUE PLOT ON THE INNER ROTOR.

TABLE V. PARAMETERS OF STATOR.

Parameter	Value	Unit
Outer radius, r_{so}	152	mm
Inner radius, r_{si}	70	mm
Air gap	3	mm
Axial length	37.5	mm
Maximum current density	7.1	A/mm^2
Winding fill factor	0.5	-

CONCLUSIONS

The 2-D magnetic design of a MSMG with a high gear ratio has been present. A flux concentration topology has been used to improve the performance. The predicted torque densities for stage 1 and stage 2 MGs are 370 Nm/L and 344 Nm/L. A magnetically geared generator has been designed by adding a stator inside the stage 2 MG. By using a MSMG the efficiency and reliability of the generator could be potentially increased thereby reducing the levelized cost of energy.

ACKNOWLEDGEMENTS

The authors would gratefully like to thank the JMAG Corporation for the use of their FEA software. This material is based upon work supported by the Hydro Research Foundation and the NC Coastal Studies Institute.

REFERENCES

[1] K. J. Binns and D. W. Shimmin, "Relationship between rated torque and size of permanent magnet machines," *IEE Proc. - Electric Power Applications,* vol. 143, no. 6, pp. 417-422, 1996.

[2] T. J. E. Miller, *Brushless Permanent-Magnet and Reluctance Motor Drives*. Oxford University Press, 1989.

[3] M. R. J. Dubois, "Optimized Permanent Magnet Generator Topologies for Direct-Drive Wind Turbines," Ph.D. Thesis, Delft University of Technology, Delft, Netherlands, 2004.

[4] K. Atallah, S. D. Calverley, and D. Howe, "Design, analysis and realisation of a high-performance magnetic gear," *IEE Proceedings - Electric Power Applications,* vol. 151, no. 2, pp. 135-143, 2004.

[5] K. K. Uppalapati, M. Calvin, J. Wright, J. Pitchard, W. Williams, and J. Z. Bird, "A Magnetic Gearbox with an Active Region Torque Density of 239Nm/L," *IEEE Trans. Ind. Appl.,* vol. PP, no. 99, pp. 1-1, 2017.

[6] P. O. Rasmussen, T. O. Andersen, F. T. Jorgensen, and O. Nielsen, "Development of a high-performance magnetic gear," *IEEE Transactions on Industry Applications,* vol. 41, no. 3, pp. 764-770, 2005.

[7] S. Miladinović, L. Ivanović, M. Blagojević, and B. Stojanović, "The development of magnetic gears for transportation applications," *Mobility & Vehicle Mechanics,* vol. 43, pp. 41-55, 2017.

[8] K. Li, J. Wright, S. Modaresahmadi, D. Som, W. Williams, and J. Z. Bird, "Designing the first stage of a series connected multistage coaxial magnetic gearbox for a wind turbine demonstrator," in *2017 IEEE Energy Conversion Congress and Exposition (ECCE)*, 2017, pp. 1247-1254.

[9] D. Som, K. Li, J. Kadel, J. Wright, S. Modaresahmadi, J. Z. Bird, and W. William, "Analysis and Testing of a Coaxial Magnetic Gearbox With Flux Concentration Halbach Rotors," *IEEE Transactions on Magnetics,* vol. 53, no. 11, pp. 1-6, 2017.

[10] N. L. Schmitz and D. W. Novotny, *Introductory Electromechanics*. Ronald Press Co., 1965.